Quantum nematic as ground state of a two-dimensional electron gas in a magnetic field

Quoc M. Doan[1] and Efstratios Manousakis[1,2]
[1]*Department of Physics and MARTECH, Florida State University, Tallahassee, Florida 32306-4350, USA*
[2]*Department of Physics, University of Athens, Penipistimiopolis, Zografos, 157 84 Athens, Greece*
(Received 19 April 2007; revised manuscript received 27 April 2007; published 22 May 2007)

We study the ground state of a nematic phase of the two-dimensional electron gas at filling fraction $\nu=1/2$ using a variational wave function having Jastrow pair correlations of the form $\Pi_{i<j}(z_i-z_j)^2$ and an elliptical Fermi sea. Using the Fermi-hypernetted-chain approximation, we find that below a critical value of the broken-symmetry parameter, the nematic phase is energetically favorable as compared to the isotropic state for the second excited Landau level. We also find that below a critical value of the layer "thickness" parameter λ (and in the actual materials), the quantum nematic is energetically favorable relative to the stripe ordered Wigner crystal phase.

DOI: 10.1103/PhysRevB.75.195433 PACS number(s): 73.43.Cd, 73.43.Lp

I. INTRODUCTION

During the past two decades, the quantum Hall effect has been one of the most intriguing research topics in condensed matter.[1] More recently, the measurements of Lilly *et al.*[2] and Du *et al.*[3] reveal a strong anisotropic behavior of transport properties of electrons for the half-filled Landau-level (LL) system under strong magnetic field and at very low temperature. The anisotropy commences at the second excited LL and persists up to the sixth excited LL. The sudden exhibition of large anisotropies of resistivities in clean two-dimensional electron gas (2DEG) suggests that there is an unknown underlying microscopic origin for this kind of spontaneous symmetry breaking.

These experimental findings prompted several interesting theoretical proposals which attempt to explain the observed anisotropic behavior of the half-filled LL system. First of all, these anisotropic transport properties are consistent with already predicted stripe and bubble charge-density-wave phases found[4,5] by means of Hartree-Fock calculations of the 2DEG. However, Fradkin and Kivelson[6] suggested that the anisotropic transport might be due to a stripe nematic phase of the 2DEG in a high magnetic field. This point of view was investigated further by Fradkin *et al.*[7] where a model for the nematic phase in a symmetry-breaking field was studied using Monte Carlo simulation. The results of the Monte Carlo simulation provide a good fit of the experimental data of Lilly *et al.*[2] This simulation suggests that the nematic phase might be a good candidate to explain the anisotropic behavior observed in Refs. 2 and 3. Furthermore, by deriving a long-wavelength elastic theory of the quantum Hall smectic state, Wexler and Dorsey[8] have estimated the transition temperature from an isotropic to nematic phase to be of the order of 200 mK. Later, Cooper *et al.*,[9] by applying an in-plane magnetic field in 2DEG samples which show the above anisotropy in transport, give further support for the possible presence of such a quantum nematic phase.

In the composite fermion theory given by Jain,[10] the fractional quantum Hall effect is interpreted as the integer quantum Hall effect of composite fermions. Furthermore, Halperin *et al.*[11] developed a theory of half-filled LL system, which is the case of our interest, as a compressible Fermi liquid. Rezayi and Read[12] proposed a ground-state wave function for the half-filled LL system having the Jastrow-Slater form as follows:

$$\Psi(\vec{r}_1,\vec{r}_2,\ldots,\vec{r}_N)=\hat{P}\prod_{j<k}^{N}(z_j-z_k)^2 \times\exp\left(-1/4\sum_{k=1}^{N}|z_k|^2\right)\det|\varphi_{\vec{k}}(\vec{r}_i)|, \quad (1)$$

where $\varphi_{\vec{k}}(\vec{r}_i)$ are two-dimensional (2D) plane-wave states, and $\hat{P}$ is the LL projector operator. Here, $z_j=x_j+iy_j$ is the complex 2D coordinate of the j electron. This wave function is a Jastrow correlated Slater determinant with Jastrow part similar to the Laughlin state.[13]

Ciftja and Wexler[14] used the Fermi-hypernetted-chain (FHNC) approximation to study a broken rotational state of the half-filled LL where the symmetry-breaking parameter was introduced in the correlation part of the wave function; namely, the Jastrow factor was modified as $\Pi_{j<k}^{N}(z_j-z_k)^2 \rightarrow \Pi_{j<k}^{N}(z_j-z_k+\alpha)(z_j-z_k-\alpha)$, and the single-particle determinant was the standard circular Fermi sea. The anisotropy symmetry-breaking parameter α is determined by minimizing the ground-state energy.

In the present paper, we adopt the ansatz for the ground state of the nematic state proposed by Oganesyan *et al.*[15] as a trial wave function in our variational calculations. The ground-state wave function proposed in Ref. 15 has the same form as the wave function given by Eq. (1); however, the single-particle momenta form an elliptical Fermi sea (Fig. 1) as opposed to the circular Fermi sea. The broken-symmetry parameter in our problem is the ratio $\alpha=k_1/k_2$ of the semimajor k_1 and semiminor k_2 axes of the elliptic Fermi sea shown in Fig. 1. We will study the nematic state of the half-filled LL system using the variational approach and we will employ the Fermi-hypernetted-chain approximation.[16–19] Namely, we investigate whether or not this state, in which the anisotropy is due to an elliptical Fermi sea, can be energetically favorable relative to the isotropic state and the stripe ordered Wigner crystal at high LL. We find that the nematic phase can be stabilized against the isotropic case

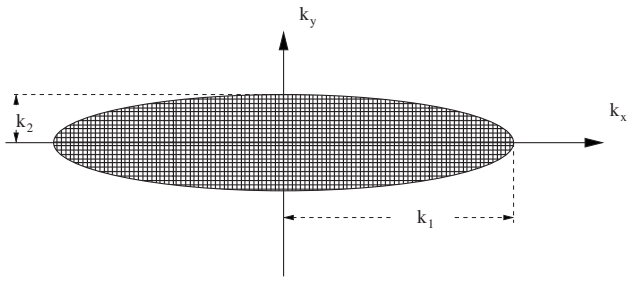

FIG. 1. The elliptic Fermi sea used in the present calculation. The vectors $\mathbf{k}=2\pi/L(n_x,n_y)$ within the shaded area denote the occupied plane-wave states which are included in the determinant. The ratio $\alpha=k_1/k_2$ is the measure of the anisotropy parameter.

beyond the second excited LL. In addition, we have compared the energy of the nematic state to that obtained by a self-consistent Hartree-Fock calculation[20] of the stripe and bubble states of the 2DEG. We find that there is a transition between the stripe ordered ground state and the nematic phase as a function of the parameter λ of the interaction used by Zhang and Das Sarma[21] to take into account the finite layer thickness. In particular, for the case of the materials[2,3] in question, we find that the ground state corresponds to the nematic state.

II. VARIATIONAL FHNC CALCULATION

The FHNC formalism for Fermi systems was introduced and developed in Refs. 16–19. A significant advantage of FHNC over the variational Monte Carlo is that FHNC does not suffer from finite-size effects. In the current problem, where we need to estimate small energy differences, the role of finite-size effects may be significant. The main idea of this method is to expand the pair distribution function in powers of the density of the system and it works well for a low-density system. The variational Monte Carlo becomes advantageous at relatively high density, as in the case of liquid ^{3}He, where the roles of the elementary diagrams and other nontrivial many-body correlations need to be included.[18]

In order to apply the FHNC formalism, first we assume that the unprojected wave function is a good approximation to the real wave function for the lowest Landau level (LLL). Moreover, it is known[22] that the projection operator almost eliminates the high LL components of the wave function. The potential energy of the high LL can be expressed[19] via the pair distribution function of the LLL using the single mode approximation discussed in Ref. 23, namely,

$$\bar{V}_L = \frac{\rho}{2}\int [g(r)-1]V_{eff}^{(L)}(r)d^2r, \tag{2}$$

where the effective potential $V_{eff}^{(L)}(r)$ at Landau level L is the convolution of the effective interaction,[21] $V(r)=e^2/\epsilon\sqrt{r^2+\lambda^2}$, with the L-order Laguerre polynomials; namely, it is the Fourier transform of

$$\tilde{V}_{eff}^{(L)}(q) = \frac{2\pi e^2}{\epsilon q}\exp(-\lambda q)[L_L(q^2/2)]^2. \tag{3}$$

In the above formula, λ is a length scale which characterizes the confinement of the electron wave function in the direction perpendicular to the heterojunction.[21]

Our calculation proceeds as follows: First, we will calculate the pair distribution functions for isotropic and nematic states with different values of the anisotropic parameter for the LLL using the FHNC approximation. Second, the interaction energies will be calculated via the pair distribution functions by using the single-LL approximation, i.e., via Eq. (2). Next, the kinetic energy is evaluated for the isotropic and different nematic states. The energy values of the isotropic state are compared with anisotropic states for the lowest, first, and second excited LLs to find out if the nematic state becomes energetically favorable. Finally, we will carry out a self-consistent Hartree-Fock calculation[20,24] for the more general case where λ can be nonzero and we will compare the energies of the nematic, isotropic, and stripe ordered Wigner crystals.

In the FHNC technique, each term in the expansion is represented as graphical diagrams with well-defined topological rules. There are nodal, composite, and elementary diagrams. In the FHNC/0 approximation, which neglects the elementary diagrams, the pair distribution function is obtained by solving the FHNC integral equations given in Ref. 18 for the case of polarized liquid ^{3}He. These equations require as input (a) the pair correlation (or Jastrow) factor, which in our case is given as $f^2(r)=\exp[u(r)]$ with $u(r)=4\ln(r)$, and (b) the statistical exchange factor $l(r)$, which for a 2D Slater determinant is given by $l(r)=C(k_Fr)$, where $C(x)\equiv 2J_1(x)/x$, $J_1(r)$ is the first-order Bessel function, and k_F is the Fermi momentum of the isotropic state. Alternatively, for the anisotropic state having an elliptic Fermi surface with major and minor axes k_1 and k_2, we find $l(\mathbf{r})=C(X)$, with $X=\sqrt{(k_1x)^2+(k_2y)^2}$, where x and y are the coordinates of $\mathbf{r}$.

Since the pseudopotential $u(r)$ has a long-range logarithmic form, we follow the standard procedure used in Ref. 1 to separate it into a short-range and a long-range part as

$$u(\mathbf{r}_{12}) = u_s(\mathbf{r}_{12}) + u_l(\mathbf{r}_{12}), \tag{4}$$

$$u_s(\mathbf{r}_{12}) = -4K_0(Qr_{12}), \tag{5}$$

$$u_l(\mathbf{r}_{12}) = 4\ln(r_{12}) + 4K_0(Qr_{12}), \tag{6}$$

where $K_0(x)$ is the modified Bessel function and Q is a wave vector which introduces a short-wavelength cutoff. The 2D Fourier transform of $u_l(r)$ is given by

$$\tilde{u}_l(\mathbf{q}) = -\frac{8\pi Q^2}{q^2(q^2+Q^2)}. \tag{7}$$

Only the *dd*-type nodal and composite functions need to be split into a short- and a long-range part:

$$N_{dd}(\mathbf{r}_{12}) = N_{dds}(\mathbf{r}_{12}) - u_l(\mathbf{r}_{12}), \tag{8}$$

$$X_{dd}(\mathbf{r}_{12}) = X_{dds}(\mathbf{r}_{12}) + u_l(\mathbf{r}_{12}). \tag{9}$$

This leads to a new set of FHNC equations for the short-range nodal and composite functions, which are solved iteratively using a combination of momentum-space and real-space approach as discussed in the Appendix.

III. RESULTS

We are interested in the potential- and total-energy difference between the isotropic ($\alpha=1$) and the anisotropic case ($\alpha>1$), namely,

$$\Delta V_L(\alpha,\lambda) = V_L(1,\lambda) - V_L(\alpha,\lambda), \tag{10}$$

$$\Delta E_L(\alpha,\lambda) = E_L(1,\lambda) - E_L(\alpha,\lambda), \tag{11}$$

as a function of λ and the anisotropy parameter α and for $L=0$, $L=1$, and $L=2$. In the interesting region, the energy difference between the nematic and the isotropic state can be small relative to the energy scale e^2/l_0, so high accuracy may be required. The effective potential for high LL and for small values of λ changes rapidly at small distances and oscillates at large distances. We have used an adaptive mesh to incorporate these multiscale oscillations accurately for up to $L=2$. For higher Landau levels, it becomes increasingly more difficult to carry out an accurate calculation due to the fact that these oscillations become increasingly more rapid.

Our calculated pair distribution function for the isotropic state accurately reproduces the pair distribution function reported in Ref. 19. The potential-energy difference $\Delta V_L(\alpha,\lambda)$ for various values of α is calculated and shown in Fig. 2 (top), in units of $e^2/(\epsilon l_0)$ (where $l_0=\sqrt{\hbar c/eB}$). Notice that for the case of the LLL and for the first excited LL, $\Delta V_L(\alpha,\lambda)<0$, i.e., the isotropic state is energetically favorable for all values of λ and α. However, as illustrated in Fig. 2 (top), for the case of the second excited LL, $\Delta V_2(\alpha,\lambda)>0$, for all values of α and for some range of the parameter λ, the anisotropic state can be energetically favorable provided that the energy loss due to the anisotropy of the Fermi surface is not larger than the potential-energy gain.

In the single-LL approximation,[23] the kinetic energy of the isotropic state is quenched. We can estimate the kinetic-energy difference between the isotropic and the anisotropic case by ignoring the Landau-level projection operator and, thus, writing the wave function as $\Psi=F\Phi$, where Φ is the noninteracting Slater determinant and F the Jastrow part. The kinetic energy contains terms in which the operator $(\nabla-\vec{A})^2$ acts on F. This term gives the same contribution of $\hbar\omega_c/2$ in both isotropic and anisotropic cases. Therefore, the main difference, coming from the term $|F|^2\Phi^*\nabla^2\Phi$, is due to the difference in shape of the Fermi sea. This leads to the following kinetic-energy difference between isotropic and anisotropic Fermi sea: $\Delta K \simeq -\frac{\hbar^2 k_F^2}{4m^*}\frac{(1-\alpha)^2}{2\alpha}$. In Fig. 2 (bottom), we present the total-energy difference $\Delta E_2(\alpha,\lambda)$ between the anisotropic and the isotropic state. Notice that the nematic state is energetically favorable relative to the isotropic below $\lambda_c \simeq 0.6$.

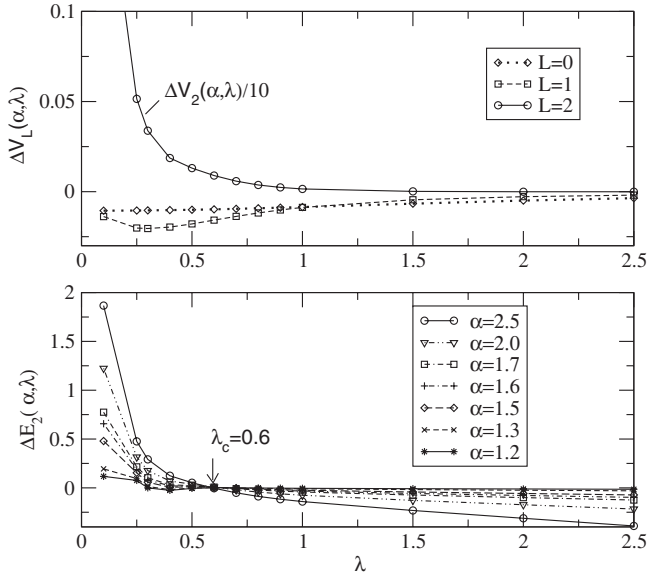

FIG. 2. Top: The potential-energy difference $\Delta V_L(\alpha,\lambda)$ as a function of λ for anisotropy parameter $\alpha=2.5$ for $L=0$, $L=1$, and $L=2$ (scaled down by a factor of 10). Bottom: The total-energy difference $\Delta E_2(\alpha,\lambda)$ as a function of λ for various values of the Fermi sea anisotropy parameter α for the second excited LL.

The results of Ref. 14 and ours share some qualitative similarities; Ciftja and Wexler found that while the ground state for the lowest LLL is isotropic, for the first and second excited LL, the anisotropic state becomes energetically favorable for a certain value of their anisotropy parameter α. In contrast, in this paper it is found that the isotropic state is still favorable for the first excited LL. This difference should be attributed to the difference between the two anisotropic wave functions: namely, the one used in the present paper has a symmetric Jastrow factor and an elliptical Fermi sea and is appropriate to model the nematic state,[15] while the wave function used in Ref. 14 has an anisotropic Jastrow factor and a circular Fermi sea.

Hartree-Fock energies of the stripe and bubble charge-density-wave energy have already been reported;[20,24] however, they are only available for the case of $\lambda=0$. In order to compare the energy of the nematic state with that of the ordered stripe and the bubble states for a nonzero value of λ, we carried out a Hartree-Fock calculation using the method outlined in Refs. 20 and 24. In Fig. 3, the total energy (apart from a common constant value of $\hbar\omega_c/2$) is compared with the results of our Hartree-Fock calculation for finite values of λ. In addition, in Fig. 4, the minimum energy with respect to the anisotropy parameter α is compared to the minimum Hartree-Fock energy value with respect to the uniaxial anisotropy parameter ϵ (the lattice constants of the uniaxial Wigner crystal are given in terms of ϵ as $a_1=\sqrt{3}a/2\sqrt{1-\epsilon}$ and $a_2=\sqrt{1-\epsilon}a/2$). Notice that there is a critical value of λ, namely, $\lambda_c \simeq 0.4$, below which the nematic phase is energetically favored.

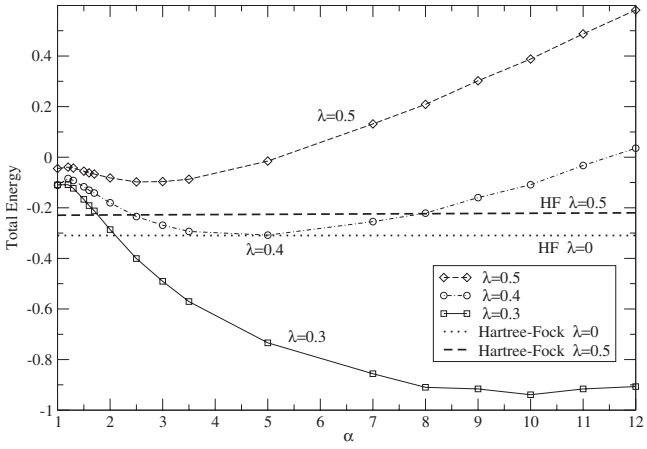

FIG. 3. The total energy as a function of the anisotropy parameter α for various values of λ.

A value for the parameter λ can be estimated using the calculation presented in Ref. 21. Using the value of the 2D electron density for these materials,[2] we find that $\lambda \sim 62$ Å. This corresponds to a value of $\lambda \sim 0.34$ in units of the magnetic length l_0 (l_0=181 Å for the value of $B \sim 2$ T, which corresponds to the second excited LL in the experiments of Refs. 2 and 3). This value of λ is less than the critical value $\lambda_c \simeq 0.4$ below which the nematic phase is energetically favorable as compared to the stripe ordered phase (see Fig. 4). Therefore, we conclude that our calculation suggests that for the case of the 2DEG in the heterojunctions used in Refs. 2 and 3 the quantum nematic state[6,7,15] may be energetically lower than the stripe ordered or bubble phases. Furthermore, it is interesting to probe this transition from the nematic to stripe to isotropic either by experimentally altering the value of λ or indirectly by means of an in-plane field.

IV. DISCUSSION

So far, because the Hartree-Fock calculations predict a stripe state, the observed anisotropy in transport was taken as

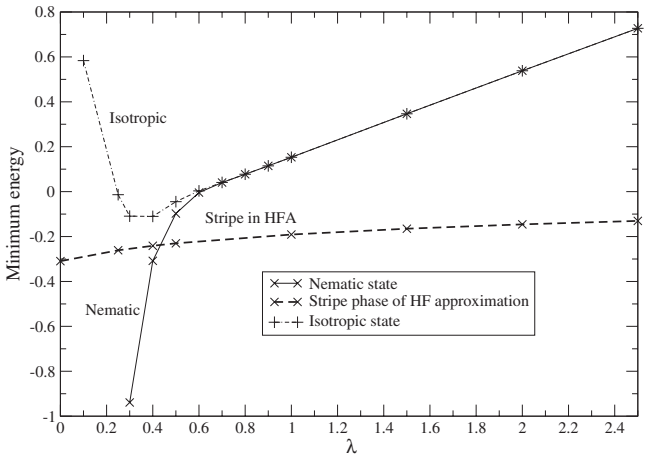

FIG. 4. The optimum values of the total energy of the nematic and isotropic states as a function of λ are compared with the results of the Hartree-Fock approximation obtained for the same values of λ.

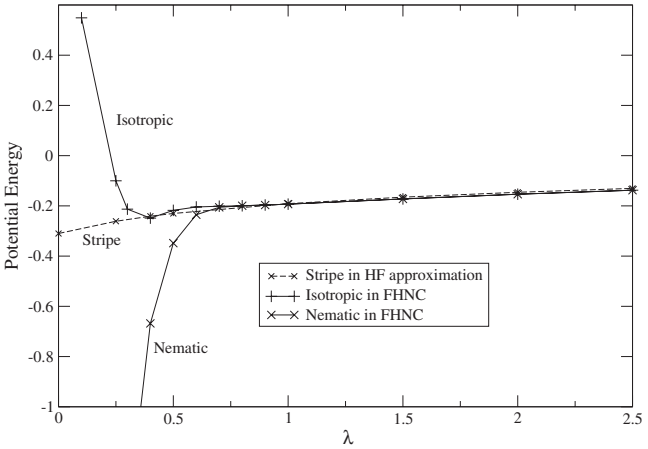

FIG. 5. The potential energies of the nematic and isotropic states as a function of λ are compared with the results of the Hartree-Fock approximation.

a signature of a stripe ordered state. This state breaks both translational invariance in one direction and rotational invariance. The results of Rezayi *et al.*[25] are also usually interpreted as a stripe state. However, the systems which can be done with such an approach are very small, and, in addition, toroidal boundary conditions were used, which break rotational invariance. Therefore, because of these limitations it cannot be discerned if the true ground state is a stripe or a nematic. In our calculation, we find that the optimum nematic phase corresponds to an anisotropy of $\alpha \sim 10$ near the physically realized value of the parameter λ. This implies that a nematic state with such large anisotropy cannot be distinguished from the stripe state in systems with only 12 electrons.[25]

There are two possible sources of systematic error in the present calculation. The first is the use of the FHNC/0 approximation to evaluate the distribution function, where the contribution of the elementary diagrams is neglected. This approximation works very well in low-density systems, i.e., where the average interparticle distance is large compared to a hard-core diameter. In the present problem, such a condition is not clearly fulfilled as there is only a soft core of size λ. The second source of error is the fact that we have neglected the projection operator and assumed that the unprojected wave function given by Eq. (1) is a good approximation to the lowest LL. In order to address these concerns, in Fig. 5 we compare only the potential energy of the nematic and isotropic states with the results of the Hartree-Fock approximation obtained for the same values of λ. Notice that for values of $\lambda > 0.6$, the results of the FHNC and the Hartree-Fock (HF) calculation are almost identical. Moreover, the results of the FHNC calculation for the isotropic state agree very well with those of the HF calculation for all values of $\lambda > 0.3$. This is an indication that the energy difference between the nematic phase and that of the isotropic state and the stripe state below $\lambda \simeq 0.5$ may not be an artifact of the difference in the treatment of the two states (i.e., the difference between HF and FHNC approximations) but rather due to the fact that the nematic state for long-range interactions is energetically favorable for at least the second excited LL.

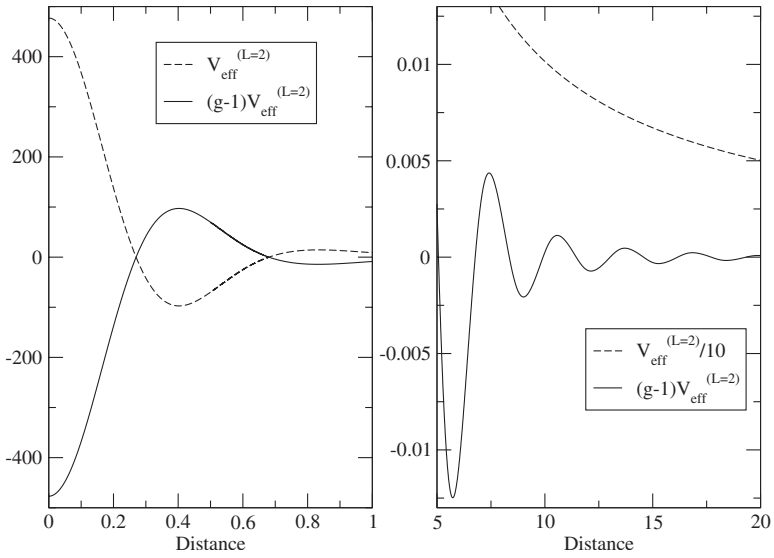

FIG. 6. The effective potentials $V_{eff}^{L=2}(r)$ (dashed line) and $(g-1)V_{eff}^{L=2}(r)$ (solid line) are shown on two different scales and ranges of r: in the range $0<r<1$ (left part of the figure) and in the range $5<r<20$ (right part of the figure).

ACKNOWLEDGMENTS

We would like to thank L. W. Engel, E. Fradkin, and S. A. Kivelson for useful discussions. This work was supported by NASA under Grant No. NAG-2867.

APPENDIX: IMPLEMENTATION OF THE FHNC

In this appendix, we discuss certain technical details applied in the FHNC iteration procedure. We find that for higher LL, we needed to solve the FHNC equations using a combination of real and momentum spaces and, in addition, a multigrid method because of the combination of the short-range large-amplitude oscillations (and, as a consequence, large cancellations) and the long-range small-amplitude oscillations.

We are interested in the energy difference [Eq. (11)] between the isotropic ($\alpha=1$) and the anisotropic case ($\alpha>1$), as a function of λ and the anisotropy parameter α and for $L=0$, $L=1$, and $L=2$. In the interesting region, the energy difference between the nematic and the isotropic state is indeed very small relative to the energy scale e^2/l_0, so very high accuracy is required in the present calculation. The effective potential [Eq. (3)] for high LL and for small values of λ changes rapidly at small distances and oscillates slowly at large distances (see Figs. 6 and 7). In Fig. 6, the quantity $F(r)=[g(r)-1]V_{eff}^2(r)$ which is integrated in Eq. (2) is shown and the integrand $rF(r)$ is also presented in Fig. 7 in order to illustrate this feature. Notice that in order to capture the short-range oscillations a very fine mesh is required, and we need to integrate up to large distances in order to capture the long-distance fluctuations. In addition, because this oscillatory behavior causes large cancellations in calculating the potential energy using Eq. (2), the energy is a small number relative to the contribution of each of the oscillations. Therefore, the small-amplitude much slower oscillations at long distances have non-negligible contribution to the small energy difference given by Eq. (11). Because these are slow and of much smaller amplitude oscillations, the long-distance contribution can be included with a wider size mesh

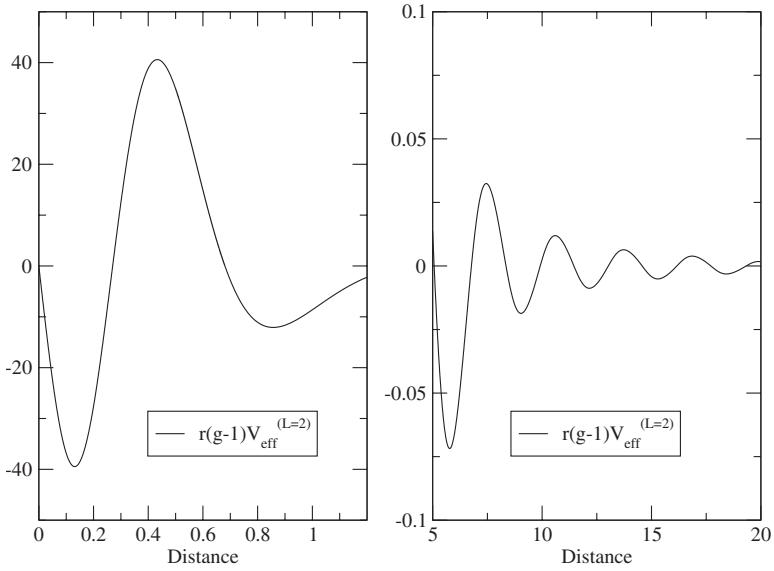

FIG. 7. The integrand $r(g-1)V_{eff}^{L=2}(r)$ used to calculate the potential energy is shown on two different scales and ranges of r: in the range $0<r<1$ (left part of the figure) and in the range $5<r<20$ (right part of the figure). Notice that there are large scale cancellations due to its rapid fluctuations at relatively small values of r and cancellations due to much longer range fluctuations due to $g-1$ at longer distances.

as compared to the grid size required for short-range oscillations. Hence, it is important to use a small enough size mesh at small distances and to include large enough distances with a much wider mesh. The FHNC equations were solved using an adaptive mesh to incorporate these multiscale oscillations accurately (see Fig. 7 and the discussion in the figure caption). In order to keep ourselves within realistic computational time scales, we needed to limit the range of our mesh size and, thus, our results can only be trusted for values of $\lambda \geqslant 0.25$.

[1] T. Chakraborty and P. Pietiläinen, *The Quantum Hall Effects Fractional and Integral*, 2nd ed. (Springer-Verlag, Heidelberg, 1995).

[2] M. P. Lilly, K. B. Cooper, J. P. Eisenstein, L. N. Pfeiffer, and K. W. West, Phys. Rev. Lett. **82**, 394 (1999).

[3] R. R. Du, H. Störmer, D. C. Tsui, L. N. Pfeiffer, and K. W. West, Solid State Commun. **109**, 389 (1999).

[4] A. A. Koulakov, M. M. Fogler, and B. I. Shklovskii, Phys. Rev. Lett. **76**, 499 (1996); M. M. Fogler, A. A. Koulakov, and B. I. Shklovskii, Phys. Rev. B **54**, 1853 (1996).

[5] R. Moessner and J. T. Chalker, Phys. Rev. B **54**, 5006 (1996).

[6] E. Fradkin and S. A. Kivelson, Phys. Rev. B **59**, 8065 (1999).

[7] E. Fradkin, S. A. Kivelson, E. Manousakis, and K. Nho, Phys. Rev. Lett. **84**, 1982 (2000).

[8] C. Wexler and A. T. Dorsey, Phys. Rev. B **64**, 115312 (2001).

[9] K. B. Cooper, M. P. Lilly, J. P. Eisenstein, L. N. Pfeiffer, and K. W. West, Phys. Rev. B **65**, 241313(R) (2002).

[10] J. K. Jain, Phys. Rev. Lett. **63**, 199 (1989).

[11] B. I. Halperin, P. A. Lee, and N. Read, Phys. Rev. B **47**, 7312 (1993).

[12] E. Rezayi and N. Read, Phys. Rev. Lett. **72**, 900 (1994).

[13] R. B. Laughlin, Phys. Rev. Lett. **50**, 1395 (1983).

[14] O. Ciftja and C. Wexler, Phys. Rev. B **65**, 205307 (2002).

[15] V. Oganesyan, S. A. Kivelson, and E. Fradkin, Phys. Rev. B **64**, 195109 (2001).

[16] S. Fantoni and S. Rosati, Lett. Nuovo Cimento Soc. Ital. Fis. **10**, 545 (1974); Nuovo Cimento Soc. Ital. Fis., A **25**, 593 (1975).

[17] E. Krotscheck and M. L. Ristig, Phys. Lett. **48A**, 17 (1974); Nucl. Phys. A **242**, 389 (1975).

[18] E. Manousakis, S. Fantoni, V. R. Pandharipande, and Q. N. Usmani, Phys. Rev. B **28**, 3770 (1983).

[19] O. Ciftja and S. Fantoni, Phys. Rev. B **58**, 7898 (1998).

[20] R. Côté, C. B. Doiron, J. Bourassa, and H. A. Fertig, Phys. Rev. B **68**, 155327 (2003); R. Côté and A. H. MacDonald, *ibid.* **44**, 8759 (1991).

[21] F. C. Zhang and S. Das Sarma, Phys. Rev. B **33**, 2903 (1986).

[22] N. Trivedi and J. K. Jain, Mod. Phys. Lett. B **5**, 503 (1993).

[23] A. H. MacDonald and S. M. Girvin, Phys. Rev. B **33**, 4009 (1986).

[24] A. M. Ettouhami, C. B. Doiron, F. D. Klironomos, R. Côté, and A. T. Dorsey, Phys. Rev. Lett. **96**, 196802 (2006).

[25] E. H. Rezayi, F. D. M. Haldane, and K. Yang, Phys. Rev. Lett. **83**, 1219 (1999).